Atmospheric Research 153 (2015) 119–133

Contents lists available at ScienceDirect

Atmospheric Research

journal homepage: www.elsevier.com/locate/atmos

Comparison of precipitation estimates between Version 7 3-hourly TRMM Multi-Satellite Precipitation Analysis (TMPA) near-real-time and research products

Zhong Liu *

Center for Spatial Information Science and Systems (CSISS), George Mason University, 4400 University Drive, Fairfax, VA 22030, USA
Goddard Earth Sciences Data and Information Services Center (GES DISC), NASA Goddard Space Flight Center, Code 610.2, Greenbelt, MD 20771, USA

ARTICLE INFO

Article history:
Received 3 March 2014
Received in revised form 24 July 2014
Accepted 31 July 2014
Available online 15 August 2014

Keywords:
Precipitation
Satellite
Remote sensing
Intercomparison

ABSTRACT

Over the years, blended methods that use multi-satellites and multi-sensors have been developed for estimating global precipitation and resulting products are widely used in applications. An example is the 3-hourly TRMM (Tropical Rainfall Measuring Mission) Multi-Satellite Precipitation Analysis (TMPA) that consists of two products: near-real-time (3B42RT) and research-grade (3B42). The former provides quick, less accurate estimates suitable for monitoring activities; the latter provides more accurate estimates more suitable for research. Both products have been widely used in research and applications. Nonetheless, to improve near-real-time applications, it is important to understand their difference. In this study, seasonal mean difference (MD), mean absolute difference (MAD), root mean square difference (RMSD), and their inter-annual variations in boreal (June, July and August or JJA) and austral (December, January and February or DJF) summers and in different rain regimes over two surface types are investigated on a large scale (50°N–50°S) from 2000 and 2012. Over land, positive MD values (3B42RT > 3B42) dominate, especially in western China, western United States, northwest Asia and over some oceanic regions of light rain in both JJA and DJF. Over ocean, negative MD values (3B42RT < 3B42) prevail, except over regions of light rain. In general, relative (to 3B42) MD values increase with rain rate. Variation of the individual differences between the two products is small (large) over regions of heavy (light) rain. There is no significant inter-annual variation in the seasonal mean statistics. The difference between the two products is likely due to the algorithms and further investigations are needed.

1. Introduction

Flood and drought events occur around the world each year, often causing heavy property damages and human casualties (i.e., Houze et al., 2011; Tripoli et al., 2005; Hoerling et al., 2013). Accurate measurements of precipitation are important for hydrologic modeling, disaster monitoring and preparedness activities. However, it is difficult to obtain observational precipitation data, especially in remote regions, continents and vast oceans where gauge and radar networks are sparse (Schneider et al., 2011, 2013; Becker et al., 2013). Satellite remote sensing techniques take an important role in filling data gaps. An example is the U.S.–Japan Tropical Rainfall Measuring Mission (TRMM), launched in November 1997, which has been providing rainfall measurements over vast under-sampled oceans and data sparse continents in the Tropics and sub-Tropics (40°N–40°S) (Garstang and Kummerow, 2000; Liu et al., 2012).

In the past three decades, satellite-derived products provide a cost-effective way to measure precipitation from space and fill in data gaps in data sparse regions. Over the years,

* Tel.: +1 301 614 5764; fax: +1 301 614 5268.
E-mail address: Zhong.Liu@nasa.gov.

http://dx.doi.org/10.1016/j.atmosres.2014.07.032

algorithms that utilize multi-satellites and multi-sensors (i.e., microwave and geostationary infrared sensors), or blended methods, have been developed to overcome a very limited spatial and temporal coverage from any single satellite (Adler et al., 2003; Huffman et al., 2007, 2009, 2010; Huffman and Bolvin, 2012, 2013; Joyce et al., 2004; Mahrooghy et al., 2012; Hong et al., 2007; Sorooshian et al., 2000; Behrangi et al., 2009; Aonashi et al., 2009) and products are widely used in hydrometeorological research and applications. For example, the TRMM Multi-Satellite Precipitation Analysis (TMPA) products (Huffman et al., 2007, 2010; Huffman and Bolvin, 2012, 2013) developed by the Mesoscale Atmospheric Processes Laboratory at NASA Goddard Space Flight Center provide precipitation estimates at 3-hourly and monthly temporal resolutions on a 0.25-degree × 0.25-degree grid available from January 1998 to present. The 3-hourly TMPA consists of two products: near-real-time (3B42RT, spatial coverage: 60°N–60°S) and research-grade (3B42, spatial coverage: 50°N–50°S). The former is less accurate, but provides quick precipitation estimates suitable for near-real-time monitoring and modeling activities (i.e., Wu et al., 2012). The latter, available approximately two months after observation, is calibrated with gauge data, different sensor calibration and additional post-processing in the algorithm. The resulting product is more accurate and suitable for research (Huffman et al., 2007, 2010). Over the years, the TMPA products have been widely used in various research and applications (i.e., Wu et al., 2012; Bitew et al., 2012; Gourley et al., 2011; Su et al., 2011; Gianotti et al., 2012).

However, issues exist in multi-satellite and multi-sensor products, as indicated by many previous studies (i.e., Tian et al., 2010; Tian and Peters-Lidard, 2010; Habib et al., 2012; Yilmaz et al., 2010; Rozante et al., 2010). For users of the near-real-time TMPA product, data quality is equally as important as the research-grade product, but limited by the availability of high quality sensor calibration and ground reference data, such as gauge data. Nonetheless, knowing their statistical differences (i.e., mean difference, mean absolute difference and root mean square difference) may help users applying the knowledge to applications by making adjustments to the near-real-time TMPA product or conducting further investigations in their areas of interest. For multi-sensor products, issues such as the entry and drop out of observing systems and post-processing procedures can create a temporal homogeneity issue affecting the quality of products as well (Huffman et al., 2007; Huffman and Bolvin, 2012, 2013). How these factors affect the statistical difference between the two TMPA products is not very clear. Huffman et al. (2007) presented a comparison result between the two daily products for a period between 1 and 4 June 2005, which is too short to understand the statistical difference. In this study, statistics derived from the two products in different rain regimes and surface types and their inter-annual variations are investigated. This article is organized as follows: Section 2 describes the data products and methods, Section 3 the results and Section 4 the conclusion and discussion.

2. Data and methods

Two TMPA products, the 3-hourly near-real-time (3B42RT) and the research-grade (3B42), are used in this study. Both products share the same 0.25-degree by 0.25-degree grid. However, the beginning dates of the two products are different. 3B42RT is available since 1 March 2000 onward and 3B42 1 January 1998; therefore the comparison in this study begins from the year of 2000 onward.

The purpose of algorithm 3B42 is to produce TRMM merged high quality (HQ) microwave/infrared (IR) precipitation and root-mean-square (RMS) precipitation-error estimates (Huffman et al., 2007, 2010; Huffman and Bolvin, 2012, 2013). 3B42 precipitation estimates are produced in four stages according to Huffman et al. (2007, 2010) and Huffman and Bolvin (2013): (1) the microwave precipitation estimates are calibrated and combined, (2) the infrared precipitation estimates are created using the calibrated microwave precipitation, (3) the microwave (HQ) and IR estimates are combined, and (4) rescaling to monthly data is applied. In addition to rescaling to monthly data, other main differences (Huffman et al., 2007, 2010) from 3B42RT (Huffman and Bolvin, 2012) are: (1) the IR calibration period in 3B42 is the calendar month in which the observation time falls, rather than a trailing 30-day accumulation in 3B42RT, and (2) the TRMM Combined Instrument (TCI) product (2B31) is used as the calibrating standard in 3B42, which should give better estimates than the TRMM Microwave Imager (TMI) by itself. Several important changes (Huffman et al., 2007, 2010; Huffman and Bolvin, 2013) have been incorporated in Version 7 3B42 and they are summarized as: (1) additional microwave products (NOAA Microwave Humidity Sounder (MHS), Special Sensor Microwave Imager-Sounder (SSMIS)), (2) a new IR dataset, the National Climatic Data Center (NCDC) GridSat-B1, has been added, (3) uniform processing of input data (AMSU, MHS, TMI, Advanced Microwave Scanning Radiometer for Earth Observing System (AMSR-E), Special Sensor Microwave/Imager (SSMI), etc.), (4) use of a single and uniformly processed gauge analysis, (5) a latitude-band calibration scheme for all satellites, and (6) additional fields in the data files (sensor-specific source and overpass time). Samples of comparison against Version 6 can be found in Huffman and Bolvin (2013).

Both Version 7 3B42RT and 3B42 are used in this study. They are archived and distributed at the NASA Goddard Earth Sciences Data and Information Services Center (GES DISC) (Liu et al., 2012). Version 7 3B42 data were downloaded from the GES DISC data search and ordering system, Mirador (http://mirador.gsfc.nasa.gov/) and the near-real-time 3B42RT from an anonymous ftp (ftp://disc2.nascom.nasa.gov/data/TRMM/Gridded/3B42RT/) at the GES DISC. There have been few processing issues before (Huffman and Bolvin, 2012, 2013), but all the products used in this study are the latest.

To facilitate product intercomparison, the GES DISC has developed prototypes in the TRMM Online Visualization and

Table 1
Rain regime classification based on rain rate (R) in two different units.

Group	A	B	C	D	E
mm/day	$R \leq 75$	$75 < R \leq 100$	$100 < R \leq 150$	$150 < R \leq 200$	$R > 200$
mm/h	$R \leq 3.13$	$3.13 < R \leq 4.17$	$4.17 < R \leq 6.25$	$6.25 < R \leq 8.33$	$R > 8.33$

Analysis System (TOVAS) (Liu et al., 2007, 2009, 2014). TOVAS (http://disc.sci.gsfc.nasa.gov/precipitation/tovas) is a member of the Geospatial Interactive Online Visualization ANd aNalysis Infrastructure (Giovanni, http://giovanni.gsfc.nasa.gov) (Liu et al., 2007; Acker and Leptoukh, 2007; Berrick et al., 2009). Giovanni is a web-based application that provides a simple and intuitive way to visualize, analyze, and access vast amounts of Earth science remote sensing data without having to download the data (Acker and Leptoukh, 2007; Berrick et al., 2009). Basic and customized comparison (i.e., scatter plot, correlation and time series) between the TMPA near-real-time and research products as well as their preceding versions can be done via either TOVAS (Liu et al., 2014) or offline analysis using customized data from TOVAS. Due to high demand for computation time and memory, all comparisons in this study were done offline.

In this study, two seasons, the boreal summer (June, July and August, JJA hereafter) and the austral summer (December, January and February, DJF hereafter), are considered since precipitation reaches the maximum amount in these two seasons in the Northern and Southern Hemispheres, respectively. Furthermore, statistics are computed separately for land and ocean in order to better observe product difference components over different surface types.

Mean difference (MD), mean absolute difference (MAD) and root mean square difference (RMSD) (Ebert, 2007) are used to measure differences between two products. If observational data are used for evaluation, MD is also equivalent to bias (Ebert, 2007). For MAD, an equal weight is given to each error. By contrast, a relatively high weight is given to RMSD because a difference is squared before averaging. In general, RMSD is greater than MAD and both of them can be used together to examine the variance in differences: the larger the difference between MAD and RMSE, the larger the variance in the individual differences in the two data sets. When MAD is equal to RMSD, there is no variation in differences. In this study, the research-grade 3B42 is treated as the "truth" due to its higher quality calibrated with gauge data over regions with good gauge coverage (Huffman et al., 2007, 2010; Huffman and Bolvin, 2012, 2013). In general, the smaller MD, MAD, and RMSD are, the

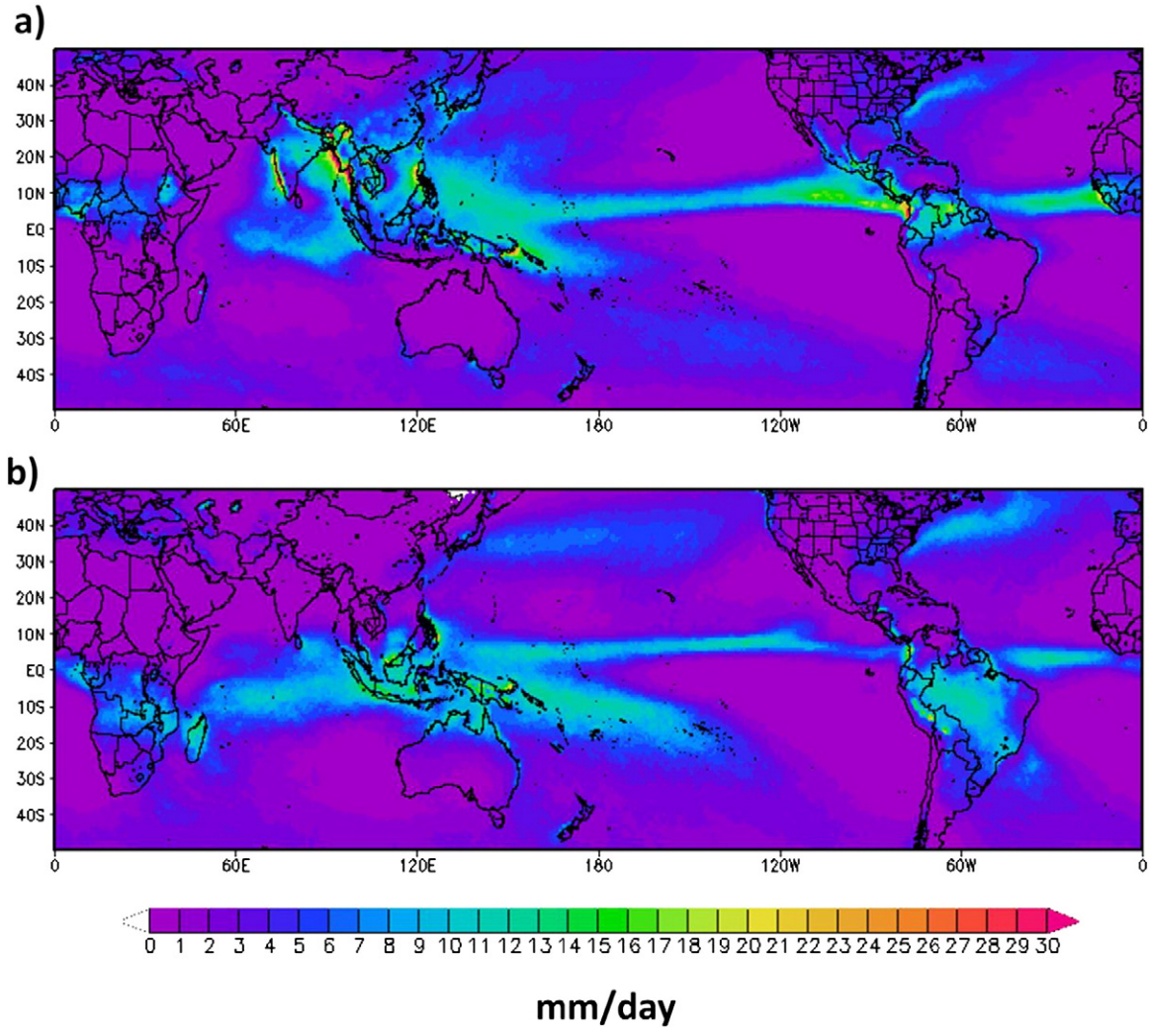

Fig. 1. Mean seasonal 3B42 precipitation estimates averaged during (a) Boreal summers (JJA) and (b) Austral summers (DJF), from 2000 and 2012.

smaller the difference is between 3B42RT and 3B42. The equations of MD, MAD and RMSD (Ebert, 2007) are written as:

$$\mathrm{MD} = \frac{1}{\mathrm{N}}\sum_{i=1}^{\mathrm{N}}(Y_i - O_i) \quad (1)$$

$$\mathrm{MAD} = \frac{1}{\mathrm{N}}\sum_{i=1}^{\mathrm{N}}|Y_i - O_i| \quad (2)$$

$$\mathrm{RMSD} = \sqrt{\frac{1}{\mathrm{N}}\sum_{i=1}^{\mathrm{N}}(Y_i - O_i)^2} \quad (3)$$

where Y_i is the estimated value of 3B42RT and O_i 3B42 at grid box i, and N is the total of samples.

The data processing is done as follows. First, MD, MAD, and RMSD for the two products are computed for each season and averaged from 2000 and 2012 at each grid point for the entire data domain (50°N–50°S). The result is presented in a map. For time series, an areal average is computed for each season and a time series plot is generated with these averages.

There is an issue for direct comparison of MD, MAD and RMSD because rain rate can vary from one grid point to another. Relative (to the mean 3B42 rain rate) MD and MAD in percentage are used, instead. In addition, the ratio between MAD and RMSD (M/R ratio hereafter) is used. As mentioned earlier, when the ratio is equal to 1, there is no variation in the individual differences. On the other hand, the smaller the ratio, the larger the variation in the individual differences.

To investigate the inter-annual variations of MD, MAD and RMSD under different rain regimes, five groups, ranging from light rain to heavy rain, are defined in Table 1. In addition, land and ocean are separated to understand the difference associated with surface types.

3. Results

3.1. General description

Figs. 1 and 2 are the mean seasonal 3B42 precipitation estimates and standard deviations for JJA and DJF, averaged from 2000 and 2012, respectively. In JJA and DJF, it is seen that

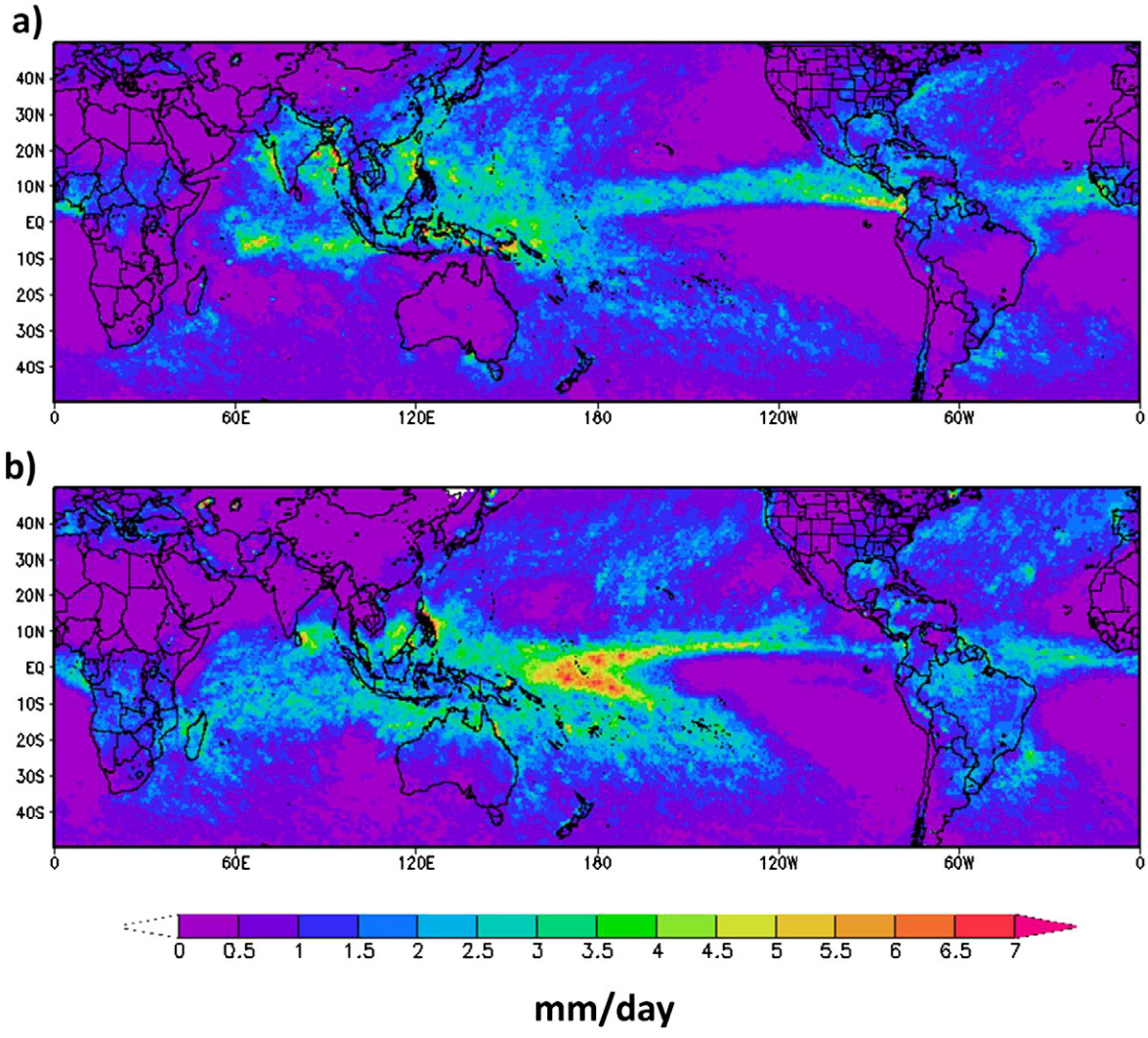

Fig. 2. Similar to Fig. 1, except for 3B42 standard deviations: (a) JJA; (b) DJF.

most of the seasonal mean rainfall is concentrated in the Tropics. Regions of heavy rain (Fig. 1a) in JJA are found in the Northern Hemisphere, near coastal mountainous regions (i.e. the southwestern coast of India, Myanmar) where the orographic effect enhances rainfall, and in the Inter-Tropical Convergence Zone (ITCZ). In DJF (Fig. 1b), regions of heavy rain

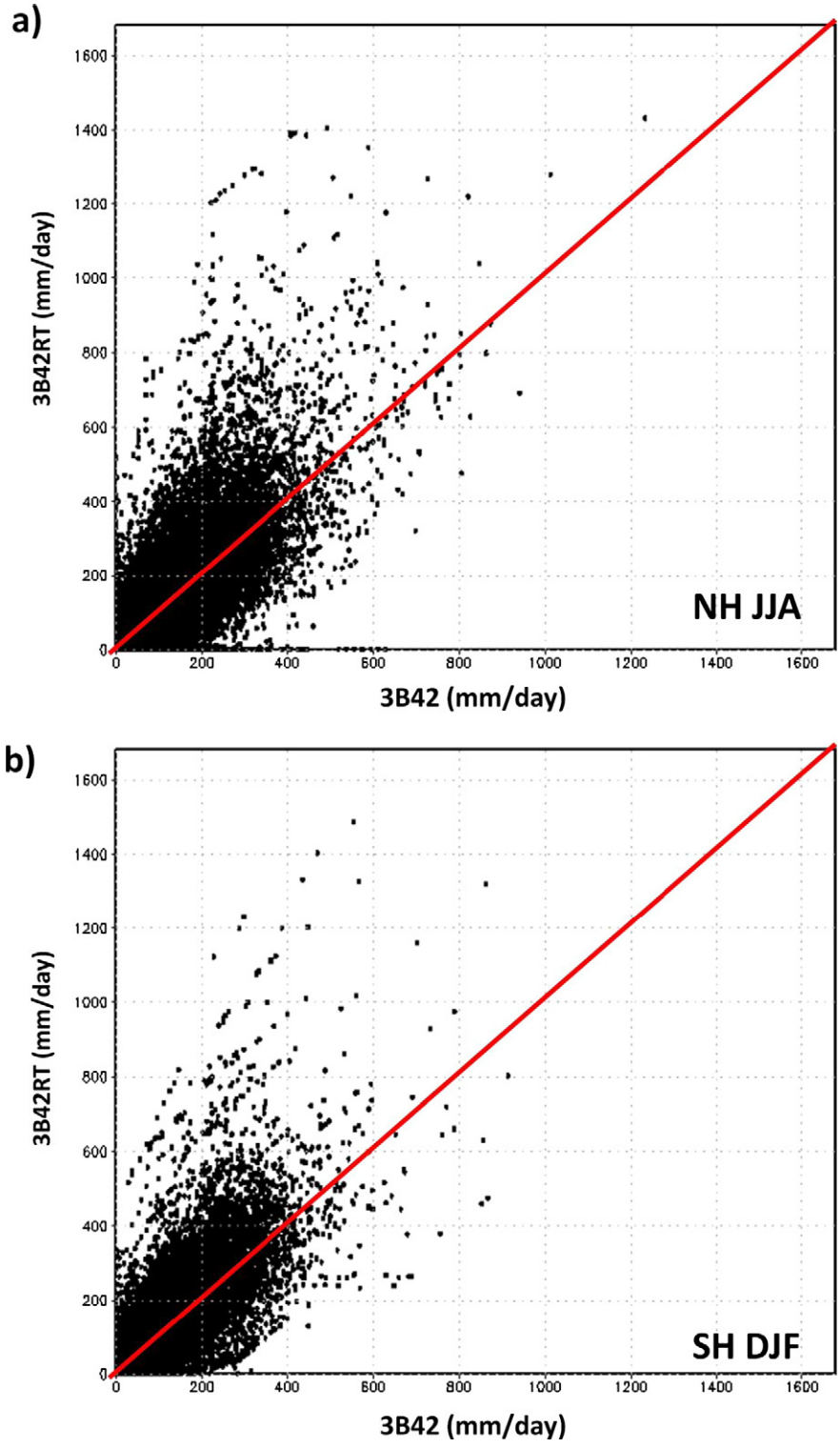

Fig. 3. Scatter plots between 3B42RT and 3B42 from 2000 and 2012: (a) Northern Hemisphere (JJA); (b) Southern Hemisphere (DJF). The redline is the 1:1 line.

are mainly found over ocean in the Southern Hemisphere. Overall, rainfall in DJF is not as heavy as in JJA. Large standard deviations are found in the regions of heavy rainfall (Fig. 2), especially in the western Pacific warm pool where the largest region of standard deviations in both JJA and DJF is found (Fig. 2b), indicating a strong inter-annual variation in rainfall amount. This variation is contributed by many factors such as the El Niño Southern Oscillation (ENSO), the Pacific Decadal Oscillation (PDO), the tropical cyclones and the Madden–Julian oscillation (MJO). Detailed discussion of such factors is beyond the scope of this study. It is also seen that several large standard deviations are found in some areas where rainfall is not heavy, such as the ocean in northeast Madagascar in JJA (Fig. 2a) and the east coast of Sri Lanka in DJF (Fig. 2b). Small standard deviations are found in light and some moderate rain regions, suggesting that the inter-annual variation there is likely to be small.

Fig. 3 contains two scatterplots of precipitation estimates for JJA in the Northern Hemisphere (Fig. 3a) and DJF in the Southern Hemisphere (Fig. 3b) from 2000 and 2012. As shown later, the difference between 3B42RT and 3B42 can change with the seasons; therefore, only the boreal and austral summers are considered and more specifically, the Northern Hemisphere is included in JJA and the Southern Hemisphere in DJF. Fig. 3 shows that both JJA and DJF are similar, but there are more heavy rain points in JJA than in DJF, which is consistent with findings in Fig. 1. There are some false alarm samples (Fig. 3), mainly in the light to moderate rain ranges, where no rain is found in 3B42RT and rain is found in 3B42, or vice versa. In a study by Huffman et al. (2007), it is concluded that the TMPA has lower skill in detecting light to moderate rain events. In Fig. 3, points are more scattered in JJA over the Northern Hemisphere than in DJF over the Southern Hemisphere, perhaps due to a large portion of land and associated gauge adjustment in the Northern Hemisphere. By contrast, a large portion of the Southern Hemisphere is dominated by ocean where gauge adjustment is not available. It is also seen that more points are found above the 1:1 line than those below in both JJA and DJF, suggesting a systematic difference in which 3B42RT has higher rainfall estimates than those of 3B42. Further analyses based on rain regimes and surface types (i.e. land vs. ocean only) are presented in Section 3.3.

Fig. 4 shows the maps of mean seasonal Pearson correlation coefficients between 3B42RT and 3B42 for JJA and DJF, respectively. Most correlation coefficients in the two maps are positive. Less than 0.7% (0.14%) of the total points in JJA (DJF) is

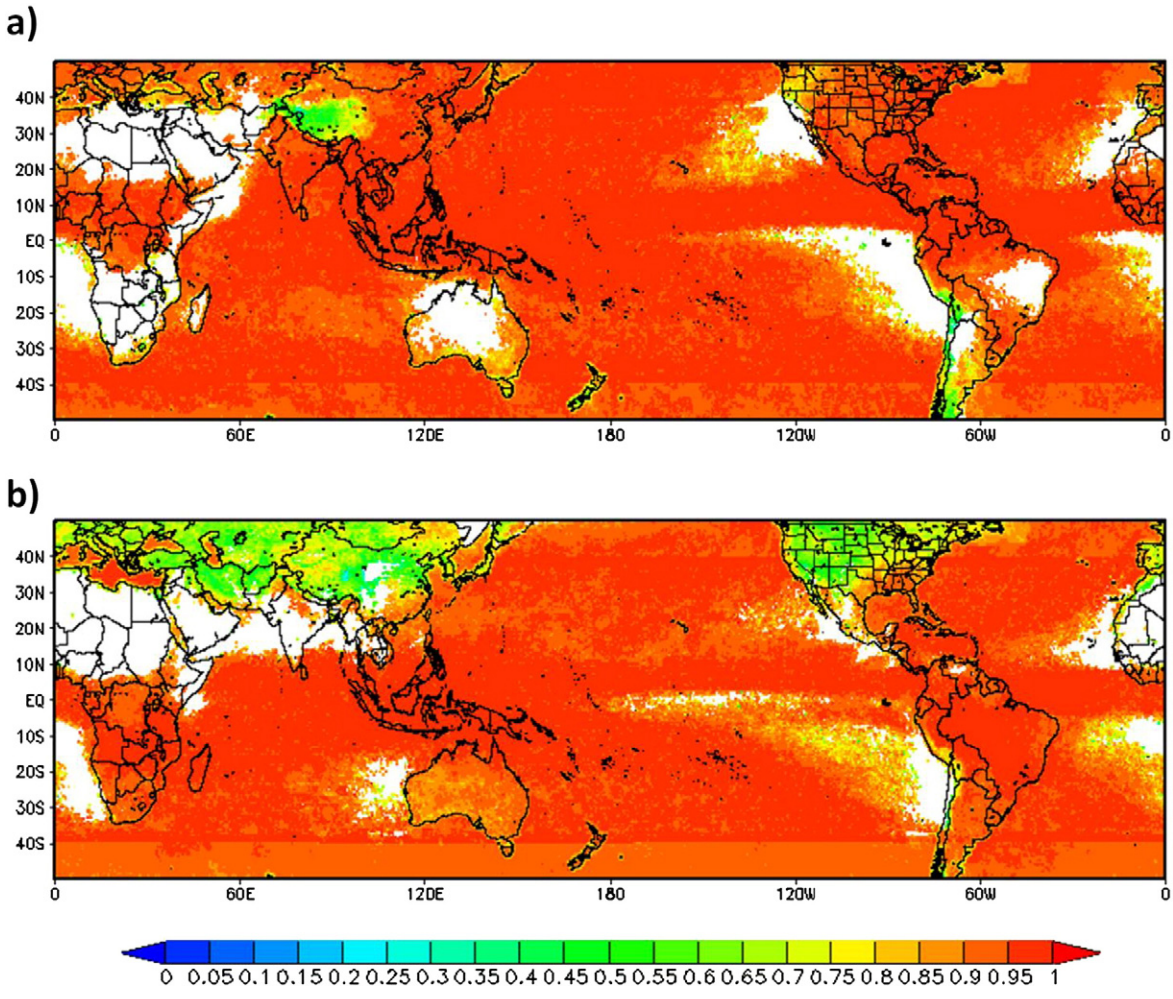

Fig. 4. Maps of mean (2000–2012) seasonal Pearson correlation coefficients between 3B42RT and 3B42 for a) JJA and b) DJF.

negative. In JJA, these negative points are scattered in western China, southern Australia whereas in DJF, the negative points are mainly located in central and western China, Iran, Turkmenistan and Uzbekistan. High coefficients (>0.95) are found in most regions, especially in areas with a high rain rate. However, smaller correlation coefficients (<0.8) are found in various places in both JJA and DJF. In JJA, the most noticeable region is the Tibetan Plateau where the coefficients (~0.5) are significantly lower than the surrounding regions (Fig. 4a). Low coefficients in JJA are found along coastlines as well, such as New Zealand, northern Japan, the Andes and south Argentina. In DJF, the most noticeable regions that have low coefficients are in the Northern Hemisphere such as western and northeastern United States, southern Europe and central Asia. It is seen that there is a discontinuity issue with correlation coefficients at 40°N and 40°S at which it is more noticeable in both JJA and DJF (Fig. 4). In short, high correlation coefficients are found in most rainy regions and low coefficients are found in mountainous regions, along coastlines, during winter and in the extratropics.

3.2. Mean seasonal relative mean difference (MD), relative mean absolute difference (MAD) and M/R ratio

Fig. 5 contains the maps of mean seasonal relative (with respect to 3B42) MD between 3B42RT and 3B42 for JJA and DJF, respectively. Small (<10%) negative values (3B42RT < 3B42) dominate the regions of heavy rain such as the ITCZ in both JJA and DJF, and the southwestern coast of India in JJA. Overall, in both JJA and DJF, positive MD values (3B42RT > 3B42) dominate over land, especially in western China, western United States, northwest Asia, etc. and over some oceanic regions of light rain as well. Over ocean, negative MD values (3B42RT < 3B42) prevail, except in some regions of light rain. The discontinuity issue previously found is here as well. In short, relative MD values over land are much larger than their means compared to those over ocean.

Fig. 6 shows the maps of mean seasonal relative MAD between 3B42RT and 3B42 for JJA and DJF. Overall, the patterns in Fig. 6 resemble those in Fig. 5: 1) smaller relative MAD values

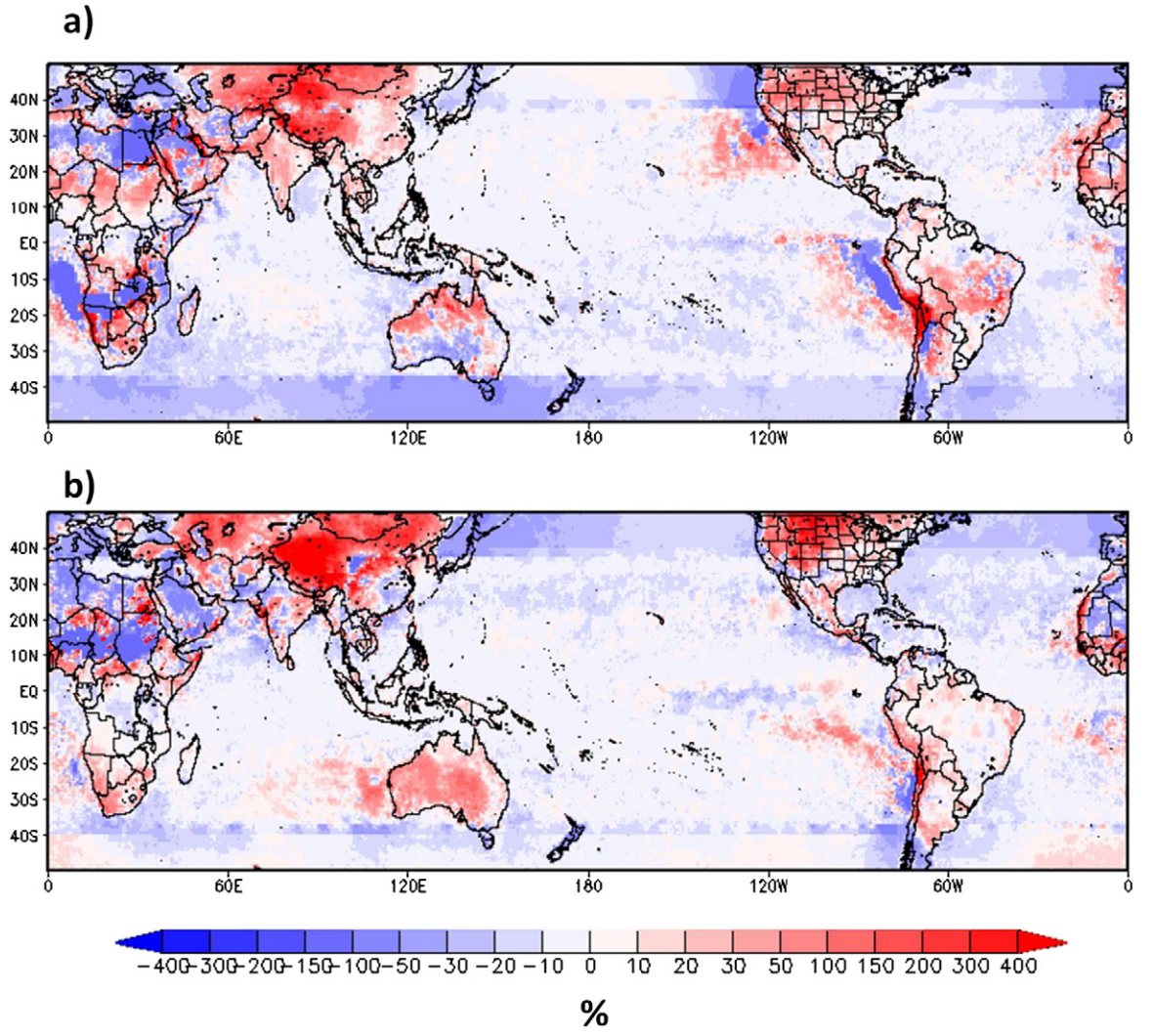

Fig. 5. Mean (2000–2012) seasonal relative (with respect to 3B42) MD between 3B42RT and 3B42 for: a) JJA and b) DJF.

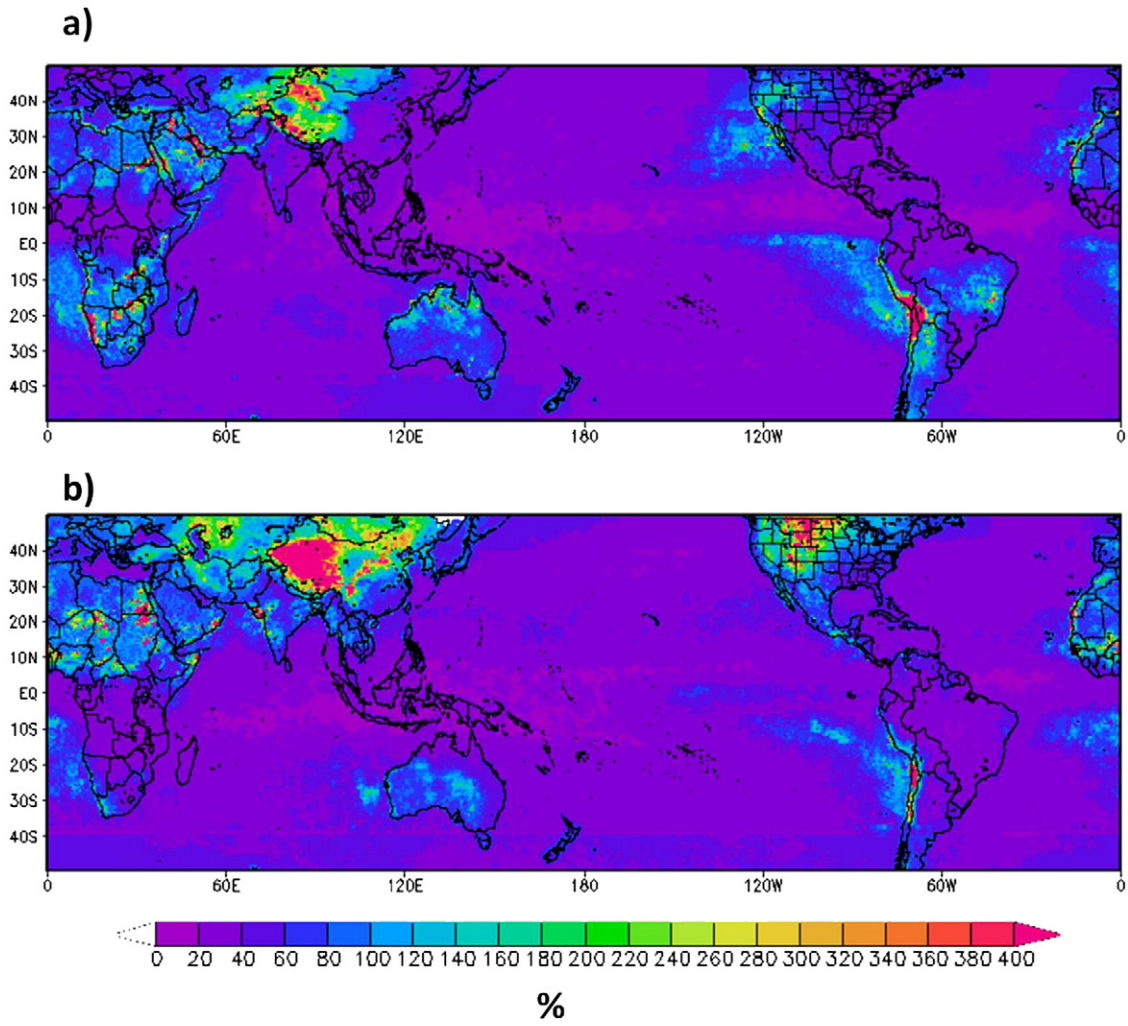

Fig. 6. Mean (2000–2012) seasonal relative MAD between 3B42RT and 3B42 for: a) JJA and b) DJF.

are found over ocean, especially over regions of heavy rain, such as the ITCZ and the southwestern coast of India and Myanmar, and 2) larger relative MAD values are found over land.

Fig. 7 shows the mean seasonal M/R ratio between 3B42RT and 3B42 for JJA and DJF, respectively. As mentioned earlier, the ratio between MAD and RMSD indicates the variance in the individual differences, namely, the smaller the ratio, the larger the variation in the individual differences. When the ratio is equal to 1, there is no variation in the individual differences. In Fig. 7, large ratios (small variation in differences) in general are found in regions of heavy rain whereas small ratios (large variation) are found in regions of light rain, such as over ocean, in northern Africa, in Australia in JJA and central Brazil in JJA. The data discontinuity issue is also found here.

3.3. Large-scale inter-annual variation of seasonal relative MD, relative MAD and M/R ratio for different rain regimes and surface types

Understanding inter-annual variations of relative MD, relative MAD and M/R ratio is important. If their variations vary randomly from year to year and have no clear patterns, it is difficult to apply adjustments to the near-real-time product (3B42RT) within applications. To help understand the difference better, only summer season is considered and in other words, only the Northern Hemisphere is included in the time series analysis in JJA and so is the Southern Hemisphere in DJF. To better understand product characteristics, land and ocean are separated in the computation as well.

Figs. 8, 9 and 10 show the time series of seasonal (JJA and DJF) averages of relative MD, relative MAD and M/R ratio over land and ocean for five different rain regimes listed in Table 1. Table 2 is the summary of the figures. In Fig. 8, it is seen that there is very little inter-annual variation in all four time series of relative MD in each group. All time series of relative MD are well defined except in Group A in which only relative MD for JJA Land is positive and all the rest remain slightly negative. Overall, relative MD for JJA Land and DJF Land (except a weak negative in Group A) is positive, suggesting a positive systematic difference (3B42RT > 3B42) over land in both seasons, which has been seen earlier. On the other hand, relative MD for JJA Ocean and DJF Ocean is negative in all groups, suggesting a negative systematic difference (3B42RT < 3B42) over ocean

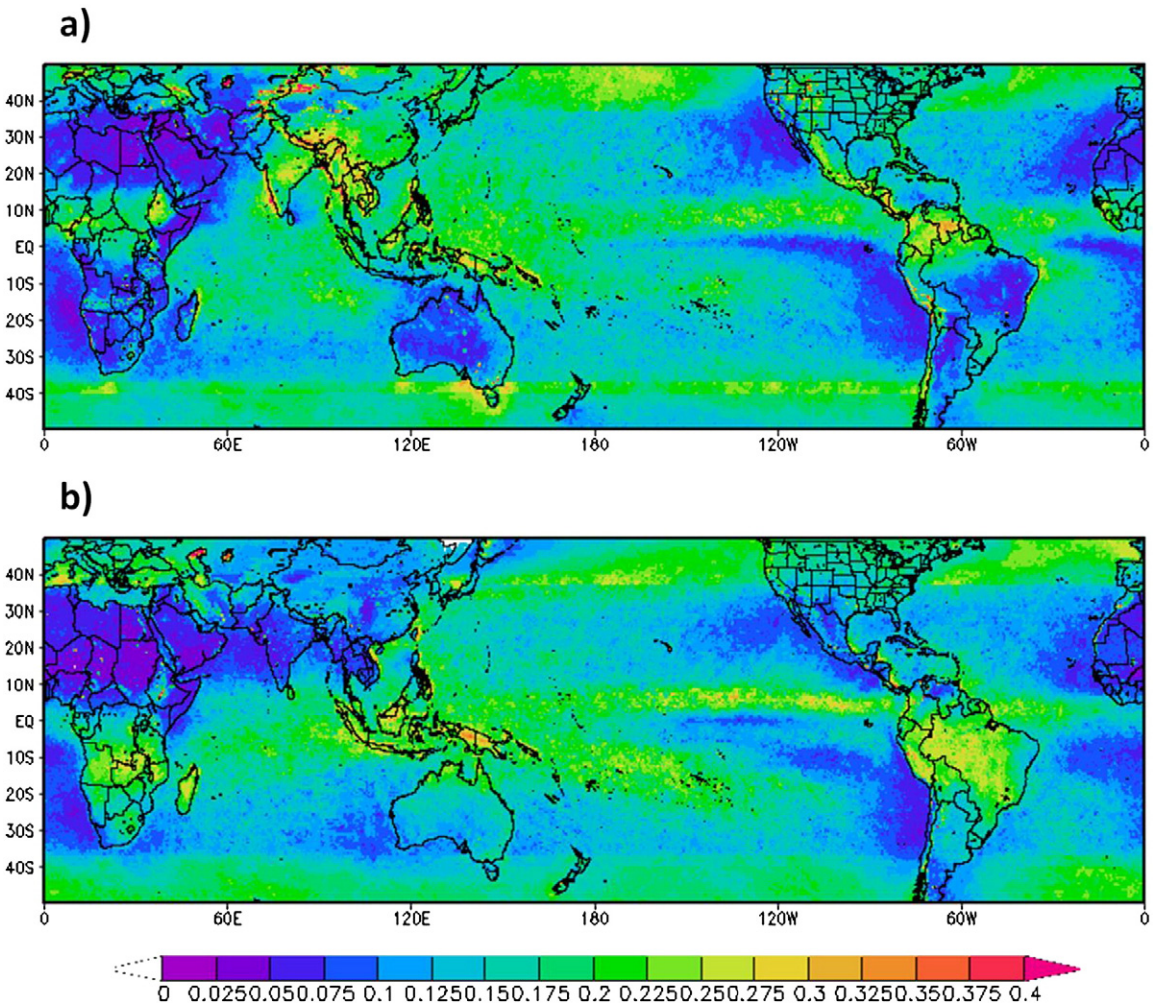

Fig. 7. Mean (2000–2012) seasonal M/R ratio between 3B42RT and 3B42 for: a) JJA and b) DJF.

between the two products. Both of these have been shown in Fig. 5 already. Relative MD values in Group A are the smallest among all of the groups. The largest relative MD values for JJA Ocean and DJF Ocean are found in Group E. Fig. 8 also shows that the systematic differences become large from Groups A to E or as rain rate increases. From Table 2, it is seen that relative MD for JJA Land is much larger than DJF Land; however, over ocean both JJA and DJF are quite similar.

Fig. 9 shows the time series for seasonal relative MAD in percentage. Like relative MD, the inter-annual variation is small. It is seen that the differences among the four time series become smaller from Group A to Group E, or as rain rate increases. For example, the range of relative MAD in Group A is approximately 25% or so, but in Group E (the last group), the range becomes around 10%. Relative MAD for JJA Land dominates from Group A to Group D. The order (JJA Land > DJF Land > DJF Ocean > JJA Ocean) exists in all groups except the last group. Relative MAD for JJA Ocean and DJF Ocean is lower than the other two over land in the first three groups. Likewise, in Table 2, relative MAD for JJA Land is larger than DJF Land, but over ocean relative MAD for DJF Ocean is larger than JJA Ocean.

Fig. 10 is the inter-annual variation of seasonal M/R ratio. Inter-annual variation is again not significant. Large variation in the individual differences is found in Group A, the smallest rain rate group, indicated by the smallest average M/R ratio (~0.21) in Table 2. This finding suggests that the variation in the individual differences for light rain is much larger than the other rain regimes. For the other groups, the average M/R ratio is greater than 0.9 and varies between 0.9 and 0.93 (Table 2) or so, suggesting small variation in the individual differences between the two products. The time series of M/R ratio are very similar in Groups C and D. M/R ratio behaves differently in each group, for example, JJA Ocean in Group A is the largest, but the smallest in Groups B to D. From Table 2, there is no significant difference among seasons and surface types.

4. Conclusion and discussion

In this study, large-scale relative MD, relative MAD, M/R ratio and their inter-annual variations in boreal and austral summers from 2000 and 2012 are investigated. Five rain regimes and two surface types are also considered.

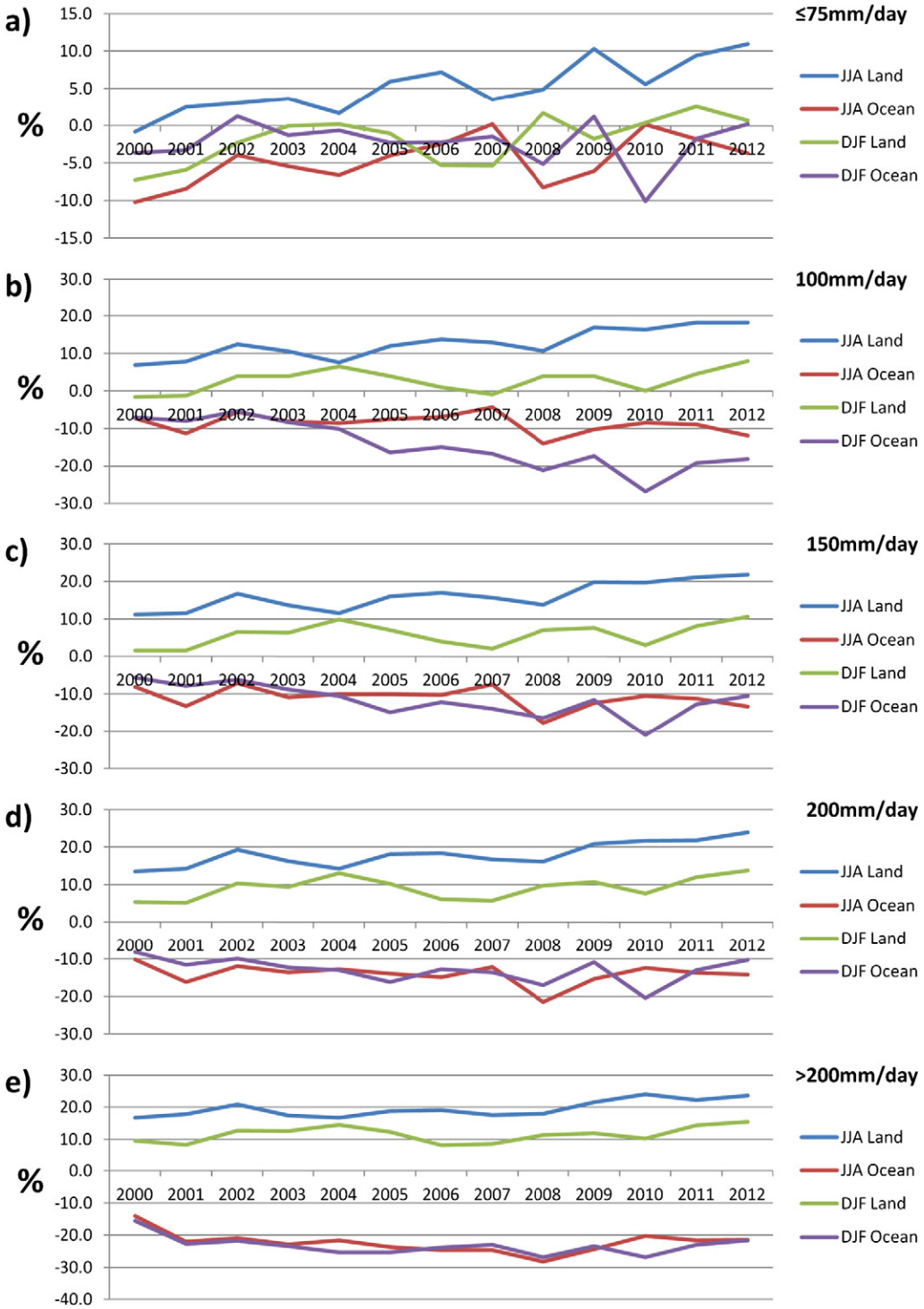

Fig. 8. Time series of seasonal relative MD.

Pearson correlation coefficients remain high in both JJA and DJF over most rainy regions, including major rain regions, such as the ITCZ and the southwestern coast of India. However, low coefficients are found in various places in both JJA and DJF. In JJA, the most noticeable region is the Tibetan Plateau where the coefficients are significantly lower than the surrounding regions. Low coefficients in JJA are found along coastlines as well, such as New Zealand, northern Japan and southern Andes. By contrast, the most noticeable regions of low coefficients in DJF (boreal winter) are in the Northern Hemisphere such as

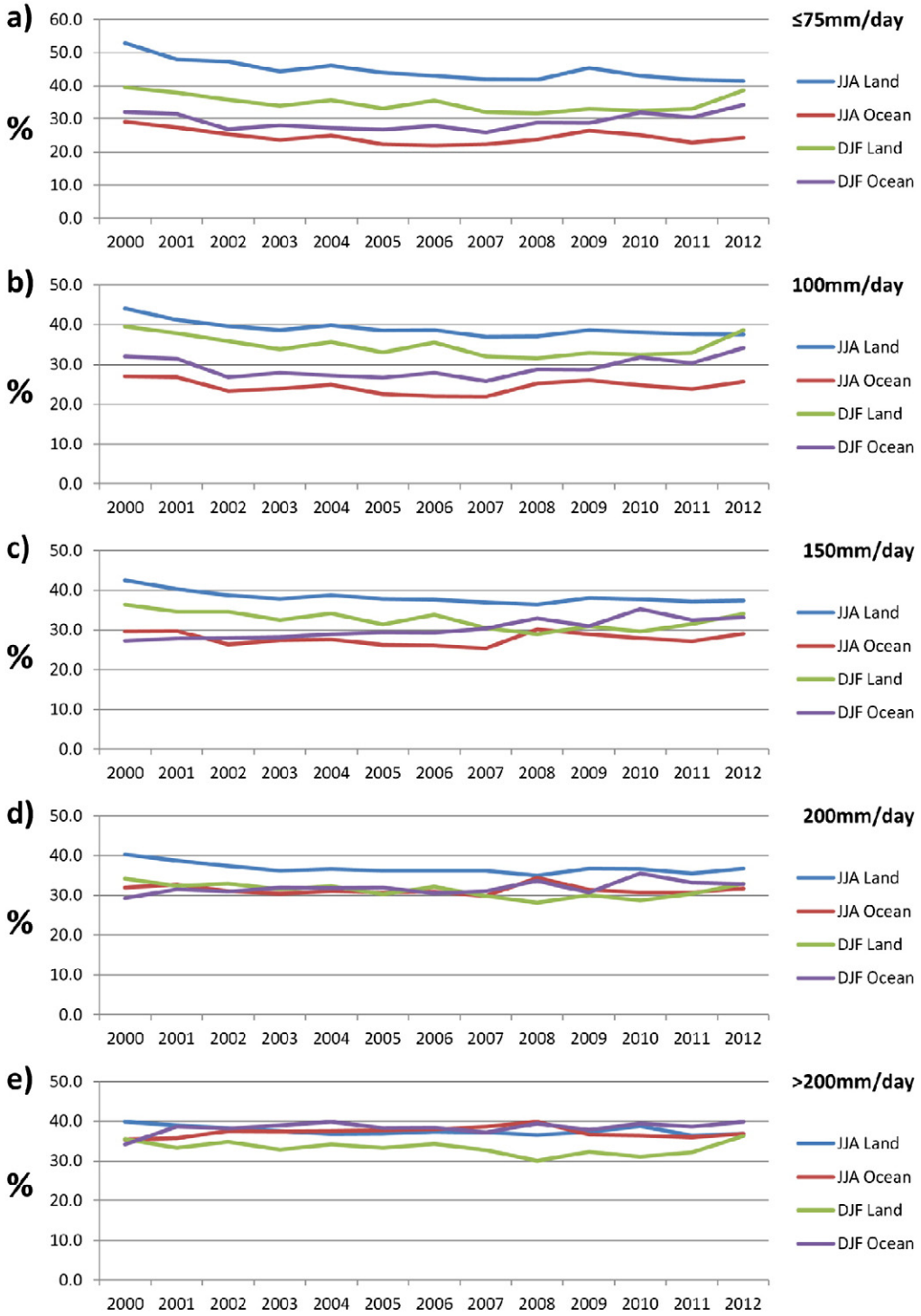

Fig. 9. Time series of seasonal relative MAD.

western and northeastern United States, southern Europe and central Asia. Based on their locations and the season, the low coefficients are perhaps related to winter precipitation type.

Relative MD changes with rain regimes and surface types. For the rain regimes in Groups B to E, well-defined positive (3B42RT > 3B42) relative MD values are found over land and negative (3B42RT < 3B42) over ocean. In general, relative MD increases with rain rate. Overall, no apparent trends are found in most relative MD time series, suggesting that adjustments to the systematic difference can be made in applications;

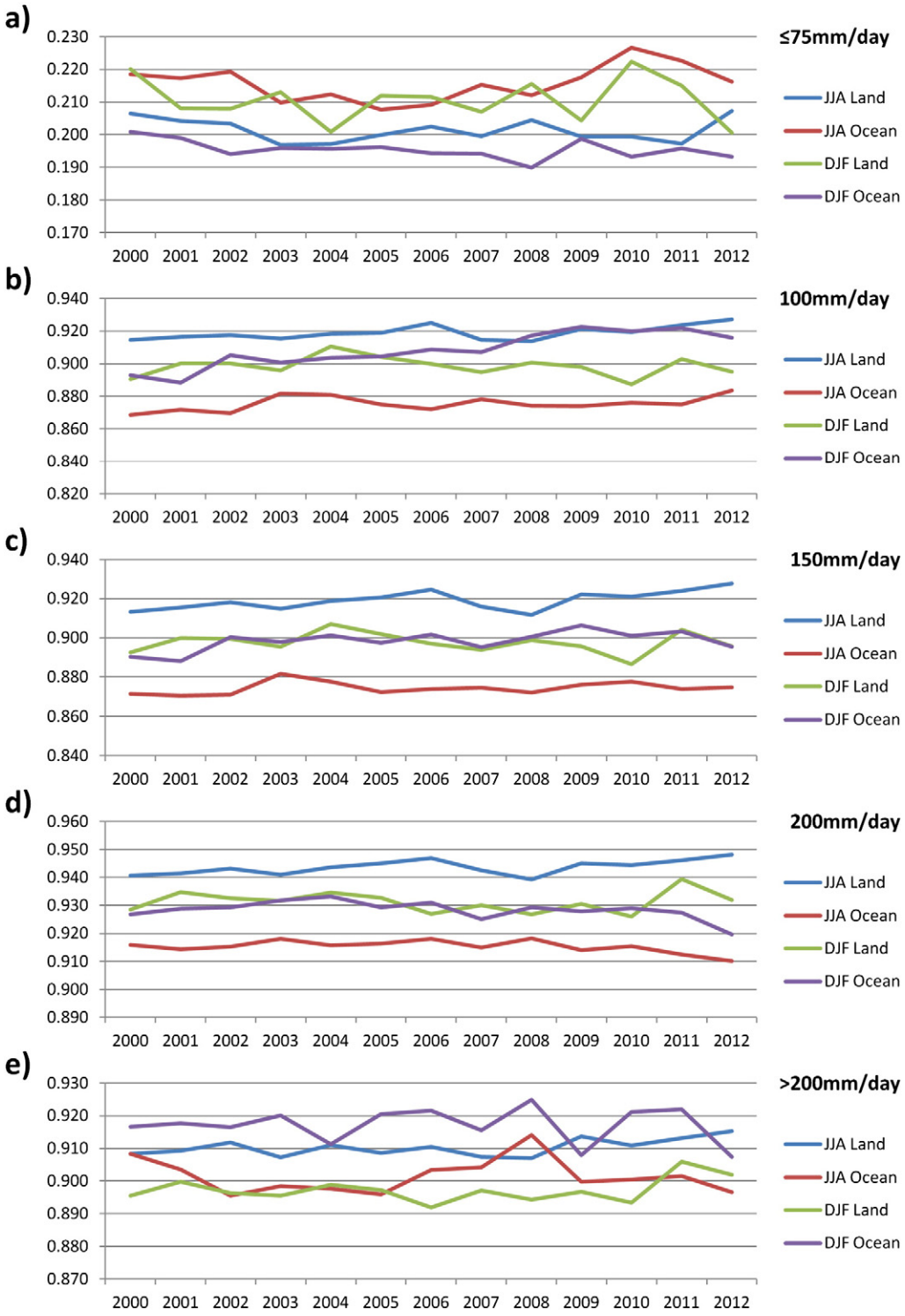

Fig. 10. Time series of seasonal M/R ratio.

however, as shown earlier, relative MD can vary in different locations due to rain regimes, surface type, terrain, season, etc. and for a specific location, a further investigation is suggested to quantify MD. Likewise, relative MAD behaves similarly to relative MD. Large M/R ratios (small variation in the individual differences) are found in regions of heavy rain and small ratio (large variation) in regions of light rain over ocean, in northern Africa, in Australia for JJA, central Brazil in JJA, etc. No apparent

Table 2
Summary of Figs. 8–10. For JJA, only the Northern Hemisphere (50°N–0°) is included and likewise, the Southern Hemisphere (0°–50°S) is included for DJF.

	Mean seasonal	JJA Land	JJA Ocean	DJF Land	DJF Ocean	Avg.
Group A	3B42 (mm/day)	1.53	2.04	2.42	1.60	1.9
	MD (%)	5.2	−4.6	−1.8	−2.2	−0.9
	MAD (%)	44.7	24.6	34.8	29.2	33.3
	M/R	0.201	0.216	0.211	0.195	0.206
Group B	3B42 (mm/day)	86.39	86.11	86.36	86.10	86.2
	MD (%)	12.7	−8.7	2.8	−14.6	−2.0
	MAD (%)	39.0	24.5	33.2	31.4	32.0
	M/R	0.919	0.875	0.898	0.908	0.900
Group C	3B42 (mm/day)	121.34	120.89	121.08	121.14	121.1
	MD (%)	16.1	−10.9	5.8	−11.7	−0.2
	MAD (%)	38.3	27.8	32.6	30.3	32.2
	M/R	0.919	0.874	0.898	0.898	0.897
Group D	3B42 (mm/day)	172.15	171.53	172.10	171.41	171.8
	MD (%)	18.1	−14.0	9.2	−13.0	0.1
	MAD (%)	36.8	31.4	31.2	31.9	32.8
	M/R	0.944	0.915	0.931	0.928	0.930
Group E	3B42 (mm/day)	292.54	262.61	291.13	257.70	276.0
	MD (%)	19.6	−22.3	11.5	−23.3	−3.6
	MAD (%)	37.6	37.2	33.3	38.4	36.6
	M/R	0.910	0.901	0.897	0.917	0.907

trend in inter-annual variation is observed as well. Gauge, different sensor calibration and other post-processing adjustments in the 3B42 algorithm (Huffman et al., 2007, 2010; Huffman and Bolvin, 2012, 2013) may be the contributing factors for the large differences in relative MD and MAD listed in Table 2. Over ocean, there is no gauge adjustment in both 3B42 and 3B42RT; however, relative MAD values are only slightly lower than those over land. In 3B42, the non-trailing IR calibration and the TCI product are used (Huffman et al., 2007, 2010; Huffman and Bolvin, 2012, 2013). In 3B42RT, a 30-day trailing IR calibration and the TMI product are used. The observed differences in this study may be associated with those adjustments.

This study has presented a statistical comparison between two popular multi-sensor and multi-satellite products. The results are complicated and vary in different locations perhaps by a combination of factors, i.e., the entry and drop-out of observing systems, sensor coverage, gauge, different sensor calibration and post-processing adjustments. It is a challenge to identify and quantify the contribution from each source and further investigations are needed. Additional fields in the data files (sensor-specific source and overpass time) may help the investigation. From Version 7, both 3B42RT and 3B42 provide such information such as IR and microwave only products, which allows the comparison of the difference between the trailing and non-trailing methods, gauge and non-gauge, and more. For example, the data discontinuity issue in Section 3.2 is likely associated with the TMI spatial coverage (40°N–40°S). In Fig. 11, the time-averaged rain rate maps show the data discontinuity issue in the microwave-based 3B41RT (Fig. 11a), the merged 3B42RT (Fig. 11b) and 3B42 (Fig. 11c). In Fig. 11a, it is seen that the discontinuity originated from 3B41RT and there is no such issue in the IR-based 3B40RT (not shown) since its coverage is between 60°N and 60°S; therefore, the discontinuity was likely carried over to the final merged product, 3B42RT (Fig. 11b). This issue seems to be fixed somehow in the final processing product 3B42 (Fig. 11c). When comparison between 3B42RT and 3B42 was conducted in this study, the discontinuity issue appeared based on this analysis. Nonetheless, further studies are needed.

This overview study is conducted on a near-global scale. By no means can the results be directly applied to error adjustments because relative MD, relative MAD and M/R ratio can vary geographically, as shown earlier. In-depth case studies in different rain regimes are needed for developing local and regional adjustments. Giovanni TOVAS (Liu et al., 2014) can provide a fast and simple way to subset data from both products for additional investigation.

Other parameters for verification, such as probability density function (PDF), probability of detection and false alarm ratio (Ebert, 2007) are also important for revealing product characteristics. More detailed information, especially on a regional or watershed scale, can be useful for hydrological modeling efforts (i.e., Wu et al., 2012) and other applications as well. Online tools (Liu et al., 2014) at the NASA GES DISC are being developed to facilitate investigations on these issues. Further categorization into coastal land and ocean can provide additional information on the characteristics of a precipitation product due to strong variation of surface emissivity, complex terrain, and other factors in coastal grid points.

Acknowledgments

This project is supported by NASA Research Opportunities in Space and Earth Science-2010 (ROSES-2010), NNH10ZDA001N-ESDRERR, Appendix A.32: “Earth System Data Records Uncertainty Analysis” and the NASA GES DISC. Special thanks to the GES DISC Giovanni development team. The TMPA data were provided by the NASA Goddard Space Flight Center's Mesoscale Atmospheric Processes Laboratory and Precipitation Processing System (PPS), which develop and compute the TMPA as a contribution to TRMM. Thanks extend to two anonymous reviewers who provided thought-provoking comments and suggestions.

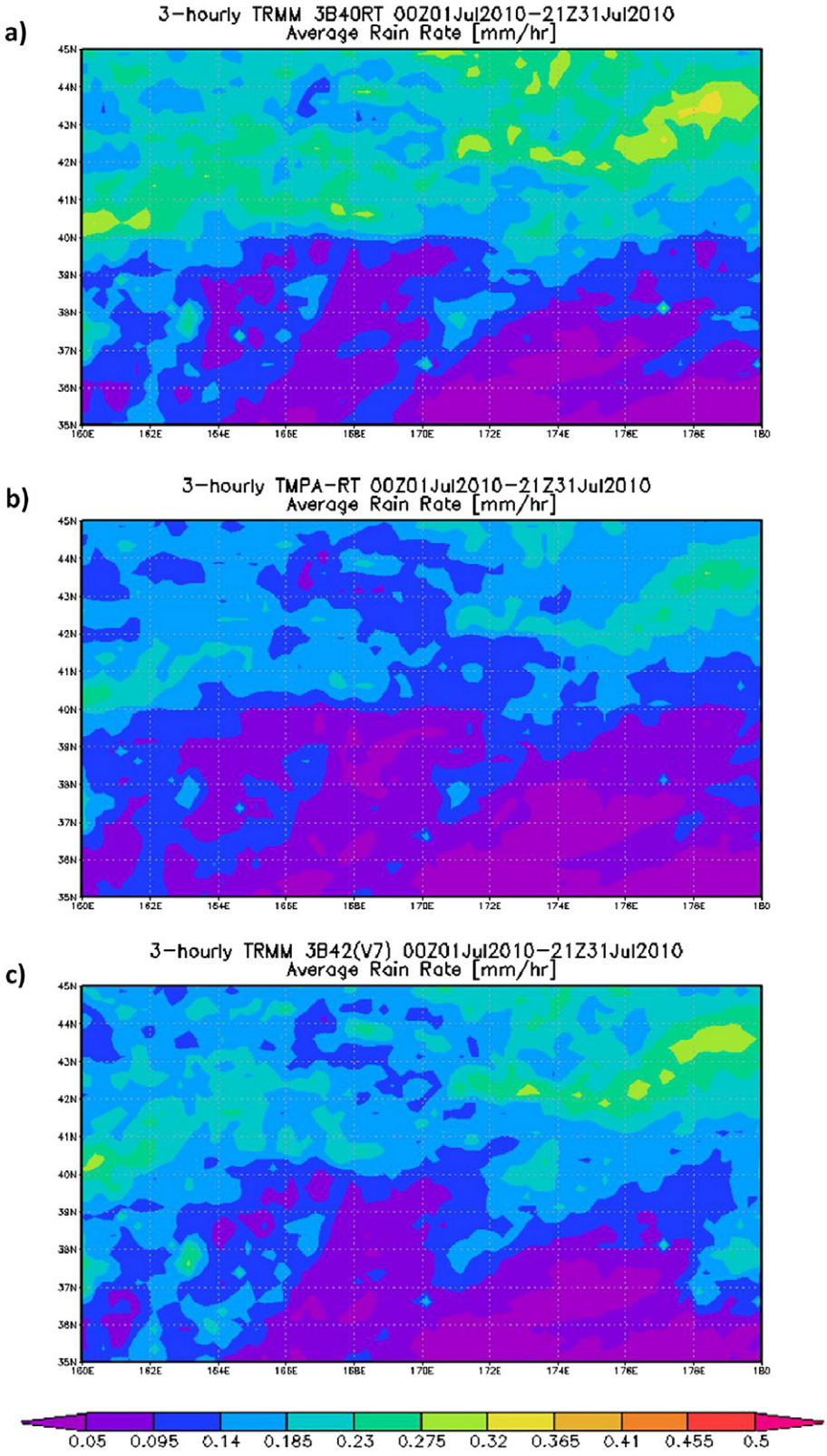

Fig. 11. Time averaged rain rate (in mm/h) maps to show the discontinuity issue in microwave-based 3B40RT (a), merged 3B42RT (b) and research-grade 3B42 (c).

References

Acker, J.G., Leptoukh, G., 2007. Online analysis enhances use of NASA earth science data. EOS Trans. Am. Geophys. Union 88 (2), 14–17.

Adler, R.F., Huffman, G.J., Chang, A., Ferraro, R., Xie, P., Janowiak, J., Rudolf, B., Schneider, U., Curtis, S., Bolvin, D., Gruber, A., Susskind, J., Arkin, P., Nelkin, E., 2003. The version 2 global precipitation climatology project (GPCP) monthly precipitation analysis (1979–present). J. Hydrometeorol. 4, 1147–1167.

Aonashi, K., Awaka, J., Hirose, M., Kozu, T., Kubota, T., Liu, G., Shige, S., Kida, S., Seto, S., Takahashi, N., Takayabu, Y.N., 2009. GSMaP passive, microwave precipitation retrieval algorithm: algorithm description and validation. J. Meteorol. Soc. Jpn 87A, 119–136.

Becker, A., Finger, P., Meyer-Christoffer, A., Rudolf, B., Schamm, K., Schneider, U., Ziese, M., 2013. A description of the global land-surface precipitation data products of the Global Precipitation Climatology Centre with sample applications including centennial (trend) analysis from 1901–present, Global Precipitation Climatology Centre, Deutscher Wetterdienst, Offenbach, Germany. Earth Syst. Sci. Data http://dx.doi.org/10.5194/essd-5-71-2013.

Behrangi, A., Hsu, K.-L., Imam, B., Sorooshian, S., Huffman, G.J., Kuligowski, R.J., 2009. PERSIANN-MSA: a precipitation estimation method from satellite-based multispectral analysis. J. Hydrometeorol. 10, 1414–1429. http://dx.doi.org/10.1175/2009JHM1139.1.

Berrick, S.W., Leptoukh, G., Farley, J.D., Rui, H., 2009. Giovanni: a web service workflow-based data visualization and analysis system. IEEE Trans. Geosci. Remote Sens. 47 (1), 106–113.

Bitew, M.M., Gebremichael, M., Ghebremichael, L.T., Bayissa, Y.A., 2012. Evaluation of high-resolution satellite rainfall products through streamflow simulation in a hydrological modeling of a small mountainous watershed in Ethiopia. J. Hydrometeorol. 13, 338–350. http://dx.doi.org/10.1175/2011JHM1292.1.

Ebert, E.E., 2007. Methods for verifying satellite precipitation estimates. Measuring Precipitation from Space — EURAINSAT and the future, Advances in Global Change Research. 28, pp. 345–356.40.

Garstang, M., Kummerow, C.D., 2000. The Joanne Simpson special issue on the tropical rainfall measuring mission (TRMM). J. Appl. Meteorol. 39, 1961. http://dx.doi.org/10.1175/1520-0450(2001)040<1961:TJSSIO>2.0.CO;2.

Gianotti, R.L., Zhang, D., Eltahir, E.A.B., 2012. Assessment of the regional climate model version 3 over the maritime continent using different cumulus parameterization and land surface schemes. J. Clim. 25, 638–656. http://dx.doi.org/10.1175/JCLI-D-11-00025.1.

Gourley, J.J., Hong, Y., Flamig, Z.L., Wang, J., Vergara, H., Anagnostou, E.N., 2011. Hydrologic evaluation of rainfall estimates from radar, satellite, gauge, and combinations on Ft. Cobb Basin, Oklahoma. J. Hydrometeorol. 12, 973–988. http://dx.doi.org/10.1175/2011JHM1287.1.

Habib, E., Haile, A.T., Tian, Y., Joyce, R.J., 2012. Evaluation of the high-resolution CMORPH satellite rainfall product using dense rain gauge observations and radar-based estimates. J. Hydrometeorol. 13, 1784–1798. http://dx.doi.org/10.1175/JHM-D-12-017.1.

Hoerling, M., Kumar, A., Dole, R., Nielsen-Gammon, J., Eischeid, J., Perlwitz, J., Quan, X., Zhang, T., Pegion, P., Chen, M., 2013. Anatomy of an extreme event. J. Clim. 26, 2811–2832. http://dx.doi.org/10.1175/JCLI-D-12-00270.1.

Hong, Y., Gochis, D., Cheng, J., Hsu, K.-L., Sorooshian, S., 2007. Evaluation of PERSIANN-CCS rainfall measurement using the NAME event rain gauge network. J. Hydrometeorol. 8, 469–482. http://dx.doi.org/10.1175/JHM574.1.

Houze, R.A., Rasmussen, K.L., Medina, S., Brodzik, S.R., Romatschke, U., 2011. Anomalous atmospheric events leading to the summer 2010 floods in Pakistan. Bull. Am. Meteorol. Soc. 92, 291–298. http://dx.doi.org/10.1175/2010BAMS3173.1.

Huffman, G.J., Bolvin, D.T., 2012. Real-Time TRMM multi-satellite precipitation analysis data set documentation. Available online ftp://trmmopen.gsfc.nasa.gov/pub/merged/V7Documents/3B4XRT_doc_V7.pdf (accessed on 8 June 2014).

Huffman, G.J., Bolvin, D.T., 2013. TRMM and other data precipitation data set documentation. Available online ftp://meso-a.gsfc.nasa.gov/pub/trmmdocs/3B42_3B43_doc.pdf (accessed on 8 June 2014).

Huffman, G.J., Adler, R.F., Bolvin, D.T., Gu, G., Nelkin, E.J., Bowman, K.P., Hong, Y., Stocker, E.F., Wolff, D.B., 2007. The TRMM multi-satellite precipitation analysis: quasi-global, multi-year, combined-sensor precipitation estimates at fine scale. J. Hydrometeorol. 8 (1), 38–55.

Huffman, G.J., Adler, R.F., Bolvin, D.T., Gu, G., 2009. Improving the global precipitation record: GPCP version 2.1. Geophys. Res. Lett. 36, L17808. http://dx.doi.org/10.1029/2009GL040000.

Huffman, G.J., Adler, R.F., Bolvin, D.T., Nelkin, E.J., 2010. The TRMM multi-satellite precipitation analysis (TAMPA). In: Hossain, F., Gebremichael, M. (Eds.), Chapter 1 in Satellite Rainfall Applications for Surface Hydrology. Springer Verlag. ISBN: 978-90-481-2914-0, pp. 3–22.

Joyce, R.J., Janowiak, J.E., Arkin, P.A., Xie, P., 2004. CMORPH: a method that produces global precipitation estimates from passive microwave and infrared data at high spatial and temporal resolution. J. Hydrometeorol. 5, 487–503.

Liu, Z., Rui, H., Teng, W., Chiu, L., Leptoukh, G., Vicente, G., 2007. Online visualization and analysis: a new avenue to use satellite data for weather, climate and interdisciplinary research and applications. Measuring Precipitation from Space — EURAINSAT and the future, Advances in Global Change Research. 28, pp. 549–558.

Liu, Z., Rui, H., Teng, W., Chiu, L.S., Leptoukh, G.G., Kempler, S., 2009. Developing an online information system prototype for global satellite precipitation algorithm validation and intercomparison. J. Appl. Meteorol. Climatol. IPWG Spec. Issue 48 (12), 2581–2589 (December 2009).

Liu, Z., Ostrenga, D., Teng, W., Kempler, S., 2012. Tropical rainfall measuring mission (TRMM) precipitation data and services for research and applications. Bull. Am. Meteorol. Soc. http://dx.doi.org/10.1175/BAMS-D-11-00152.1.

Liu, Z., Ostrenga, D., Teng, W., Kempler, S., Milich, L., 2014. Developing GIOVANNI-based online prototypes to intercompare TRMM-related global gridded-precipitation products. Comput. Geosci. 66, 168–181.

Mahrooghy, M., Anantharaj, V.G., Younan, N.H., Aanstoos, J., Hsu, K.-L., 2012. On an enhanced PERSIANN-CCS algorithm for precipitation estimation. J. Atmos. Ocean. Technol. 29, 922–932. http://dx.doi.org/10.1175/JTECH-D-11-00146.1.

Rozante, J.R., Moreira, D.S., de Goncalves, L.G.G., Vila, D.A., 2010. Combining TRMM and surface observations of precipitation: technique and validation over South America. Weather Forecast. 25 (3), 885–894 (June 2010).

Schneider, U., Becker, A., Meyer-Christoffer, A., Ziese, M., Rudolf, B., 2011. Global precipitation analysis products of GPCC. Available online ftp://ftp-anon.dwd.de/pub/data/gpcc/PDF/GPCC_intro_products_2008.pdf (accessed on 10 September 2013).

Schneider, U., Becker, A., Finger, P., Meyer-Christoffer, A., Ziese, M., Rudolf, B., 2013. GPCC's new land surface precipitation climatology based on quality-controlled in situ data and its role in quantifying the global water cycle, Global Precipitation Climatology Centre, Deutscher Wetterdienst, Offenbach, Germany. Theor. Appl. Climatol. http://dx.doi.org/10.1007/s00704-013-0860-x.

Sorooshian, S., Hsu, K.-L., Gao, X., Gupta, H.V., Imam, B., Braithwaite, D., 2000. Evaluation of PERSIANN system satellite-based estimates of tropical rainfall. Bull. Am. Meteorol. Soc. 81, 2035–2046. http://dx.doi.org/10.1175/1520-0477(2000)081<2035:EOPSSE>2.3.CO;2.

Su, Fengge, Gao, Huilin, Huffman, George J., Lettenmaier, Dennis P., 2011. Potential utility of the real-time TMPA-RT precipitation estimates in streamflow prediction. J. Hydrometeorol. 12, 444–455. http://dx.doi.org/10.1175/2010JHM1353.122.

Tian, Y., Peters-Lidard, C., 2010. A global map of uncertainties in satellite-based precipitation measurements. Geophys. Res. Lett. 37 (L24407), 1–6. http://dx.doi.org/10.1029/2010GL046008.

Tian, Y., Peters-Lidard, C., John, B., 2010. Real-Time bias reduction for satellite-based precipitation estimates. J. Hydrometeorol. 11, 1275–1285. http://dx.doi.org/10.1175/2010JHN1246.1.

Tripoli, G.J., Medaglia, C.M., Dietrich, S., Mugnai, A., Panegrossi, G., Pinori, S., Smith, E.A., 2005. The 9–10 November 2001 Algerian flood: a numerical study. Bull. Am. Meteorol. Soc. 86, 1229–1235. http://dx.doi.org/10.1175/BAMS-86-9-1229.

Wu, H., Adler, R.F., Hong, Y., Tian, Y., Policelli, F., 2012. Evaluation of global flood detection using satellite-based rainfall and a hydrologic model. J. Hydrometeorol. 13, 1268.1284.

Yilmaz, K., Adler, R., Tian, Y., Hong, Y., Pierce, H., 2010. Evaluation of a satellite-based global flood monitoring system. Int. J. Remote Sens. 31, 3763–3782. http://dx.doi.org/10.1080/01431161.2010.483489.